

## Euclid Quick Data Release (Q1) - Spectroscopic search, classification and analysis of ultracool dwarfs in the Deep Fields

C. DOMINGUEZ-TAGLE,<sup>1,2</sup> M. ŽERJAL,<sup>1,2</sup> N. SEDIGHI,<sup>1,2</sup> P. MAS-BUITRAGO,<sup>3</sup> E. L. MARTIN,<sup>1,2</sup>  
J.-Y. ZHANG,<sup>1,2</sup> N. VITAS,<sup>1,2</sup> V. BEJAR,<sup>1,2</sup> S. TSILIA,<sup>1,2</sup> S. MUÑOZ TORRES,<sup>1,2</sup> N. LODIEU,<sup>1,2</sup>  
D. BARRADO,<sup>3</sup> E. SOLANO,<sup>3</sup> P. CRUZ,<sup>3</sup> R. TATA,<sup>4</sup> N. PHAN-BAO,<sup>5,6</sup> AND A. BURGASSER<sup>7</sup>

<sup>1</sup>*Instituto de Astrofísica de Canarias, La Laguna, Spain*

<sup>2</sup>*Universidad de La Laguna, Dpto. Astrofísica, La Laguna, Spain*

<sup>3</sup>*Centro de Astrobiología (INTA-CSIC), Villanueva de la Cañada, Madrid, Spain*

<sup>4</sup>*Department of Physics and Astronomy, Ohio University, USA*

<sup>5</sup>*Department of Physics, International University, Ho Chi Minh City, Vietnam*

<sup>6</sup>*Vietnam National University, Ho Chi Minh City, Vietnam*

<sup>7</sup>*Department of Astronomy & Astrophysics, UC San Diego, USA*

### ABSTRACT

The Near-Infrared Spectrometer and Photometer onboard the *Euclid* space mission has obtained near-infrared (NIR) slitless spectra of millions of objects, including hundreds of ultracool dwarfs. *Euclid* observations retrieve images and spectra simultaneously. This observing mode marks a new era in the discovery of new objects, such as L- and T-type dwarfs, which can be found from direct identification through the H<sub>2</sub>O and CH<sub>4</sub> absorption bands. NISP spectral resolution ( $R \sim 450$ ) is enough to classify the objects by the spectral type using known standard templates. Q1 provided more than 4 million NIR spectra in one visit to the Euclid Deep Fields. The large amount of spectra released in these fields allowed us to: a) confirm almost half of the UCD photometric candidates by J. Y. Zhang et al. (2024); b) discover at least 10 new late L- and T-type dwarfs searching directly in the spectra database; and c) spectroscopically confirm one hundred more candidates from a new photometric selection conducted by M. Žerjal et al. (2025). We present a preliminary list of *Euclid* UCD templates built by the combination of the best spectra from all these searches. We include the first spectral analysis of confirmed UCDs from Q1 data; spectral classifications; determination of effective temperatures; H<sub>2</sub>O, CH<sub>4</sub> and NH<sub>3</sub> spectral indices; and measurements of the KI absorption doublet. This paper is a first step in the study of *Euclid* UCDs and will be improved with each subsequent data release.

*Keywords:* Surveys (1671) — Brown dwarfs (185) — Late-type dwarf stars (906) — T dwarfs (1679) — Spectroscopy (1558)

### 1. INTRODUCTION

The advent of the *Euclid* space mission (Y. Euclid Collaboration: Mellier et al. 2024)

is expected to foster major advancements in many fields of astrophysics. The *Euclid* Quick Data Release (Q1) includes slitless near-infrared (NIR) spectra of 4.3 million objects

observed with the Near-Infrared Spectrometer and Photometer (NISP; [K. Euclid Collaboration: Jahnke et al. 2024](#)). Among those millions of sources, several hundred are UCDs, which have effective temperatures below 2700 K ([J. D. Kirkpatrick et al. 1995](#)) and down to  $\sim 250$  K for the coldest object observed to date ([K. L. Luhman 2014](#); [K. L. Luhman et al. 2024](#)). The spectral classification system for UCDs follows their decreasing temperatures: late M-type (M7 and later, [J. D. Kirkpatrick et al. 1997](#), L-type ([E. L. Martín et al. 1997, 1998, 1999](#); [J. D. Kirkpatrick et al. 1999, 2000](#)), T-type ([A. J. Burgasser et al. 2002](#); [T. R. Geballe et al. 2002](#); [A. J. Burgasser et al. 2006](#)), and Y-type dwarfs ([P. Delorme et al. 2008](#); [M. C. Cushing et al. 2011](#); [J. D. Kirkpatrick et al. 2011](#)).

This paper focuses on the spectroscopic capabilities of *Euclid* in the field of UCD science, and is part of a collection of papers dedicated to the study of ultracool dwarfs. Here we investigate whether NISP’s spectral resolution and sensitivity are sufficient to analyze the molecular bands of H<sub>2</sub>O, CH<sub>4</sub> and NH<sub>3</sub> (see [E. L. Martín et al. 2021](#)), as well as other spectral features, in order to classify them and to study their physical properties. To this end, we focus on four objectives:

- To confirm the photometric UCD candidates published by [J. Y. Zhang et al. \(2024\)](#), through the analysis of *Euclid* spectra.
- To discover new late-L and T-type UCDs by directly searching in the spectra database.
- To confirm the photometric UCD candidates selected from Q1 data by [M. Žerjal et al. \(2025\)](#).
- To classify the UCD candidates by spectral type and to investigate the determination of effective temperatures, spectral indices,

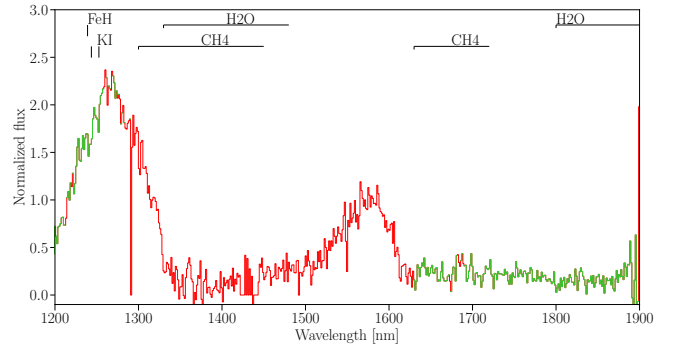


**Figure 1.** Spectrum of E597913, a T7 object from Zhang’s compilation with spectra available in Q1 data. The flux is normalized at 1600 nm. The spectrum is plotted without any smoothing. The green lines represent the spectra with NDITH > 2 and the red lines indicate the values with QUALITY < 0.7.

pseudo-equivalent widths of the KI absorption doublet, and the possibility of identifying objects with unusual high radial velocities.

*Euclid* observations retrieve visible and NIR images and NIR spectra simultaneously, using its two instruments VIS ([M. Euclid Collaboration: Cropper et al. 2024](#)) and NISP in a Reference Observing Sequence (ROS; [R. Euclid Collaboration: Scaramella et al. 2022](#)). Each ROS includes four images in the four bands ( $I_E$ ,  $Y_E$ ,  $J_E$ , and  $H_E$ ) and four spectra by performing a dithering pattern. The four dithering positions (Level-1 data) can be coadded to increase the signal-to-noise ratio (SNR) and to eliminate unwanted artifacts (cosmic rays, bad pixels, optical ghosts, etc.). For most of the *Euclid* survey, only one ROS is planned, with the exception of the Euclid Deep Fields (EDFs), which will be observed repeatedly during the mission. These deep fields are grouped in three regions North, Fornax and South: EDF-N, EDF-F, and EDF-S, respectively.

Q1 ([H. Aussel et al. 2025](#)) provides calibrated data of one visit to the EDFs. The data include coadded and calibrated images and extracted spectra, as well as catalogs for the different type of objects (stars, galaxies, etc.). Q1 data in-

clude 4.3 million extracted NISP spectra which cover the wavelength range 1200 to 1900 nm (see Y. *Euclid* Collaboration: Copin et al. 2025; V. Le Brun et al. 2025). The spectra files include wavelength (in air), flux density, the flux density variance, along with the following flags<sup>8</sup>:

**NDITH:** number of individual spectra combined for this pixel.

**MASK:** a bit mask for the current pixel signaling saturation, ghost, persistence, etc. The specific bit meaning is included in the header of the DQ extension of each SIR spectrogram.

**QUALITY:** a number between 0 and 1 that represents the ratio between the weighted sum of the pixels combined and the weighted sum of all the pixels.

While slitless spectra observing mode provides the spectrum of every object in the field of view, there is a significant probability of contamination among the objects. In addition, given that NISP has a mosaic of 16 detectors with gaps between them, all or part of the object spectrum could fall into these gaps for some of the dithering positions (out of four in a single ROS). An example of a Q1 spectrum of E597913 (alias composed by the first 6 digits of the *Euclid* ID) of a confirmed T7 UCD in the EDF-N identified by J. Y. Zhang et al. (2024) is shown in Fig. 1. The spectrum is displayed in two colors: green lines represent the spectra with NDITH > 2 and red lines represent the spectra with QUALITY < 0.7. The number of dithering positions can change with wavelength, so plotting the spectrum in two colors helps identify any unreliable portions (i.e. from unidentified contamination). We chose the value of 0.7 for QUALITY as it filters most of the artifacts. Future data releases will be based on the

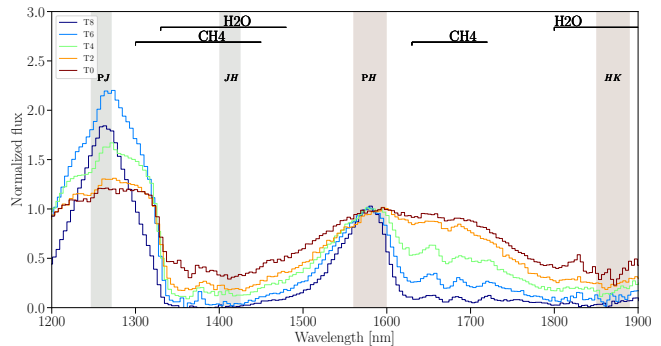


**Figure 2.** Spectral regions used for the spectroscopic search, plotted over the spectra of the T-dwarf standard templates (references in Appendix A).

combination of more dithering positions, so that QUALITY and NDITH values will increase.

This paper is organized as follows: Sect. 2 describes the photometric candidates and the non-photometric search of late L- and T-type objects in Q1 data; Sect. 3 describes the spectroscopic confirmation and classification; Sect. 4 shows the preliminary *Euclid* UCD templates; Sect. 5 reviews the spectral analysis of the confirmed UCDs; and Sect. 6 presents our conclusions.

## 2. RETRIEVING UCD CANDIDATES FROM Q1 DATA

Two photometric catalogs and one direct search are the main input to this work:

- The photometric catalog of J. Y. Zhang et al. (2024, hereafter Zhang’s compilation) is a selection of previously known objects filtered to find UCD candidates. Spectroscopically confirmed UCDs in this work are identified as “UCD benchmarks”.
- The spectroscopic search of late L- and T-type objects in the 4.3 million spectra.
- The photometric catalog of Žerjal et al. (in prep., hereafter Žerjal’s catalog) which has been prepared using the UCD benchmarks.

<sup>8</sup> <http://st-dm.pages.euclid-sgs.uk/data-product-doc/dm10/>

### 2.1. Zhang’s compilation

In preparation for *Euclid* observations, J. Y. Zhang et al. (2024) performed a photometric selection of UCDs in the region of the EDFs, and published a list of 515 candidates. They selected eight candidates which they confirmed as UCDs by obtaining reconnaissance spectra from the 8.2-m Very Large Telescope (VLT) and 10.4-m Gran Telescopio Canarias (GTC). Five of the objects from this selection are found in Q1 data (our alias in parentheses): WISEA J035909.75–474056.8 (E597913), WISEA J035231.80–491059.4 (E581332), WISEA J033234.35–273333.8 (E531434), WISEA J040254.85–470440.9 (E607287), and WISEA J175730.71+674138.4 (E269377).

Zhang’s compilation includes NIR photometry from the Two Micron All Sky Survey (2MASS; R. M. Cutri et al. 2003; M. F. Skrutskie et al. 2006). In this work we label these photometric measurements with the “2MASS” suffix (e.g.,  $J_{2\text{MASS}}$ ) to differentiate from NISP photometry ( $Y_E$ ,  $J_E$ , and  $H_E$ ).

**Table 1.** New late-L and T dwarfs found by the spectroscopic search algorithm.

Alias	SpT	$PJ-JH$	$PH-JH$	$PH-HK$
E528241	T5	0.9	0.7	0.7
E265716	T4?	0.9	0.9	0.9
E523574	T4	0.9	0.8	0.8
E273062	T3	0.9	0.8	0.6
E536416	T2	0.8	0.8	0.8
E273015	T1	0.8	0.8	0.8
E644720	T1?	0.7	0.6	0.6
E511520	T0	0.8	0.8	0.9
E267056	L9	0.7	0.7	0.5
E517518	L9	0.6	0.6	0.5

NOTE— The third to fourth columns are the search indices defined in the text. The spectral type (SpT) is described in Sect. 3.3.

### 2.2. Spectroscopic search for late-L and T dwarfs

Given that Zhang’s compilation had a very low number of late L- and T-type candidates, and that Q1 data released 4.3 million spectra, we decided to search for the accentuated spectral features of late-L and T dwarfs directly in the spectra database without any photometric analysis. In particular, the combined absorption of  $\text{H}_2\text{O}$  and  $\text{CH}_4$  is so evident in the spectral range covered by NISP that a fast algorithm computing ratios can easily detect these absorption bands. We developed an algorithm that filters the data to eliminate unreliable values using `QUALITY` and `NDITH` flags and computes three ratios from four narrow spectral regions. The values for these regions were adapted from the NIR spectral indices defined by A. J. Burgasser et al. (2006), to the expected *Euclid* spectra of T dwarfs. These regions are plotted together with four T-dwarf standard templates in Fig. 2. The regions are labeled as  $PJ$  and  $PH$  for the peak regions, and  $JH$  and  $HK$  for deepest region of the water absorption bands. We selected these regions because *Euclid* observations are free from telluric absorption bands. The search algorithm normalize the integrated fluxes over the regions to the peak values and computes three ratios  $PJ-JH$ ,  $PH-JH$ , and  $PH-HK$ . It works in two steps, first with the spectra free from unreliable values, then for the spectra convolved with a gaussian profile. In both cases it filters by the minimum values of 0.6 and 0.5 for  $PJ-JH$  and  $PH-JH$ , respectively. In the second step it filters by  $PH-HK > 0.35$ . We calibrated these values running the search algorithm on the spectra of known T dwarfs. We ran the search algorithm over the entire database with satisfying results. The output included numerous spectra filled with contamination from other sources that resembled portions of expected spectral energy distribution. After a visual inspection, we kept the best findings,

which turned into 10 new UCDs not published before. Table 1 list these 10 objects discovered by the search algorithm, and gives the values of the search indices. This table includes their spectral type, described in Sect. 3.1. It is interesting to see that the 10 objects spectral types span homogeneously from L9 to T5. The objects retrieved by the algorithm that were not discoveries, are described in Sect. 3.3.

### 2.3. Žerjal’s catalog

One of the main advantages of *Euclid* observations is the simultaneous retrieval of images and spectra. This observing mode marks a new era in catalog creation, because the point-source filtering criteria can be tuned based on the immediate spectroscopic confirmation (Žerjal et al. in prep.). While this confirmation can be limited by the spectrograph sensitivity or availability, the selection criteria can be extrapolated to the rest of objects, reaching the photometric limiting magnitudes. Using the UCD benchmarks and the direct-search T-type objects to verify the selection criteria, M. Žerjal et al. (2025) created a catalog with more than 5000 UCD candidates. The photometric selection could be biased and limited by the sensitivity of the VIS instrument as described in the same paper.

## 3. SPECTROSCOPIC CONFIRMATION AND CLASSIFICATION

### 3.1. Spectral type (*SpT*) classification

We classified the objects by comparing the spectra to the standard templates compiled in SPLAT (A. J. Burgasser & Splat Development Team 2017), and selecting the spectral type by the best fit in the full wavelength range. Appendix A gives the details of the standard templates employed. The result for a selection of the best quality spectra (few artifacts and high signal to noise, where possible) for each spectral subclass is plotted in Fig. 3 to show the spectral sequence. These spectra are plotted with-

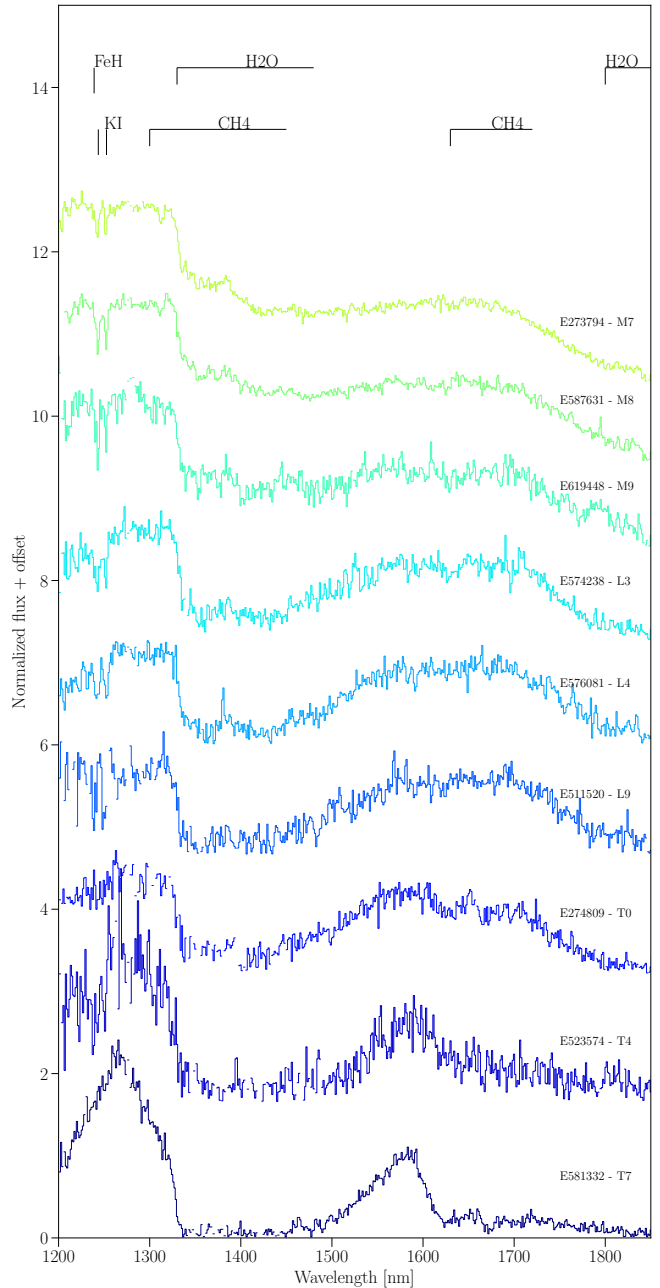


**Figure 3.** Spectral sequence for objects from M7 to T7 that shows *Euclid*’s ability to observe UCDs. The flux is normalized at 1600 nm. The spectra are plotted without any smoothing. The missing values are due to artefact removal.

out any smoothing. The missing values are due to artefact removal (as shown in red in Fig. 1).

### 3.2. Spectra for Zhang’s compilation

We searched for Zhang’s compilation of UCD candidates in the Q1 released spectra using their

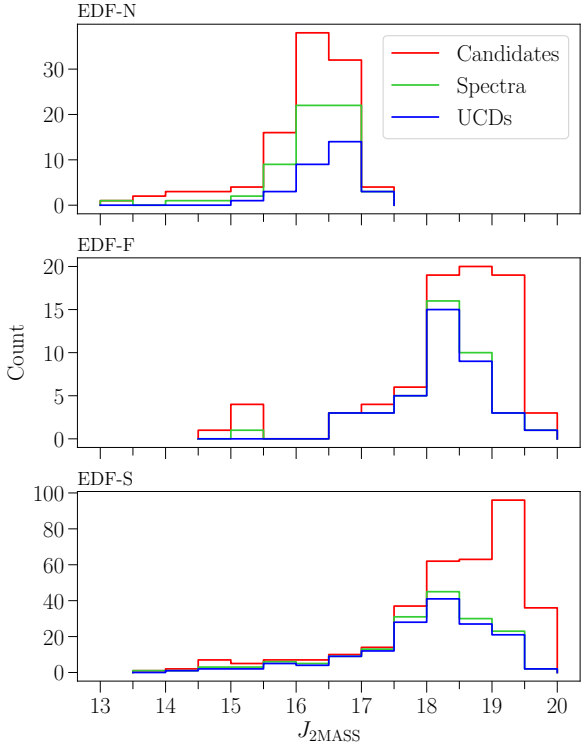


**Figure 4.** Histogram of Zhang’s compilation divided by field, EDF-N (top), EDF-F (mid), and EDF-S (bottom). The y-scale is expanded for the latter. Each plot includes all the candidates (red line), the dwarfs confirmed by Q1 spectra (green line) and the UCDs (blue line).

**Table 2.** Number of cross-matched objects between Q1 data and Zhang’s compilation).

Field	Zhang candidates	Q1 cross-matched to 1''	Q1 cross-matched 1 - 2.5''	Confirmed dwarfs	Confirmed UCDs
EDF-N	89	64	22	61	30
EDF-S	348	319	28	178	155
EDF-F	78	75	2	42	39

NOTE—The fourth column indicates the number of matches increasing the search radius. The fifth column gives the total number of dwarfs confirmed. The sixth column gives the number of confirmed dwarfs classified as UCDs.

object coordinates. Out of 4.3 million spectra, we found 458 objects matching within 1 arcsecond and 52 objects matching within 1 to 2.5 arcsecond of the coordinates. Together, these 510 objects account for 99% of Zhang’s compilation. An exhaustive comparison of these spectra with standard templates allowed us to confirm 224 UCDs. Table 2 shows the number of cross-matched objects, the number of confirmed dwarfs and the number of UCDs among them. In the case of EDF-N the confirmed UCDs represent 35% of the candidates with available spectra, given the limited depth of Zhang’s compilation in this field. These numbers represent a minimum, as we excluded some candidates from confirmation owing to the poor SNR of their spectra. Future visits to the EDFs will allow us to increase the total number of confirmations. Fig. 4 shows the distribution of the number of objects per  $J_{2MASS}$  magnitude. The histograms are divided by field (North, South, and Fornax) to show the objects confirmed spectroscopically in each case. Note that from Zhang’s compilation, EDF-N is the more limited field in magnitude. The UCDs with the best fits to the standard templates (negligible fit residuals) are selected as the “UCD benchmarks”. There are 60 objects in this list, 38 late-M dwarfs, 19 L dwarfs, and 3 T dwarfs with magnitudes  $14 \leq J_{2MASS} \leq 19$ . Table 6 in Appendix B provides the full list.

The rest of the confirmed objects include 55 peculiar late M- and L-dwarfs, 70 with large residuals and 39 that look like L dwarfs but cannot be reliably classified at the moment. The latter group of objects must wait for future visits to the EDFs which will allow a better classification, as the survey will gradually gain an additional depth of 2 magnitudes upon completion (Y. Euclid Collaboration: Mellier et al. 2024).

Fig. 5 shows the spectra of E535151, the faintest L1 UCD from Zhang’s compilation

found in Q1 data, together with that of E654087, the brightest L1 UCD from the same compilation. For this spectral type the span goes from  $15.1 \leq J_{2MASS} \leq 18.6$ .

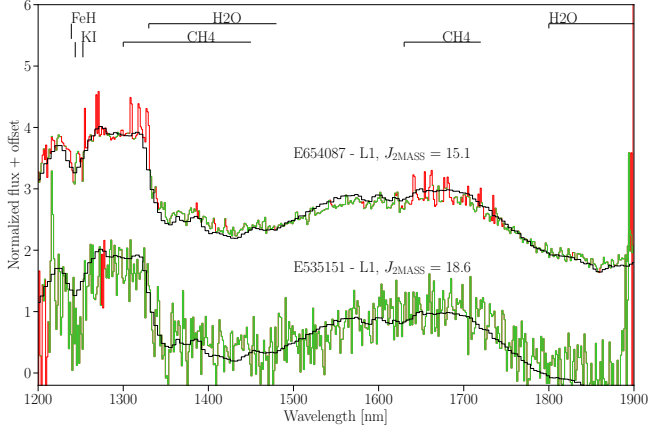


**Figure 5.** The brightest and faintest L1 UCDs from Zhang’s compilation (E654087 and E535151, respectively). The flux is normalized at 1600 nm. The green lines represent the spectra with  $NDITH > 2$  and the red lines indicate the values with  $QUALITY < 0.7$ . The black lines represent the L1 standard template (A. J. Burgasser et al. 2004).

### 3.3. Spectra retrieved by the spectroscopic search algorithm

The 10 new UCDs discovered by the search algorithm were spectroscopically classified and their SpT is included in Table 1. There is one UCD for each spectral subtype, from L9 to T5. There are also two objects, E644720 and E265716, that have a peculiar spectral energy distribution (signaled with a “?” symbol), as shown in Fig. 6. E265716 could be a binary not revealed by the images, owing to its peculiar spectrum that fits to a T4 in the  $J$ -band and T2 in  $H$ -band. We are investigating this possibility. There are 5 additional T dwarfs found by the algorithm that were already known: one from Zhang’s compilation, two found by Žerjal’s et al. (in prep.) in the process of creating their photometric catalog, one from G. N. Mace et al. (2013), and one found as a QSO contaminant

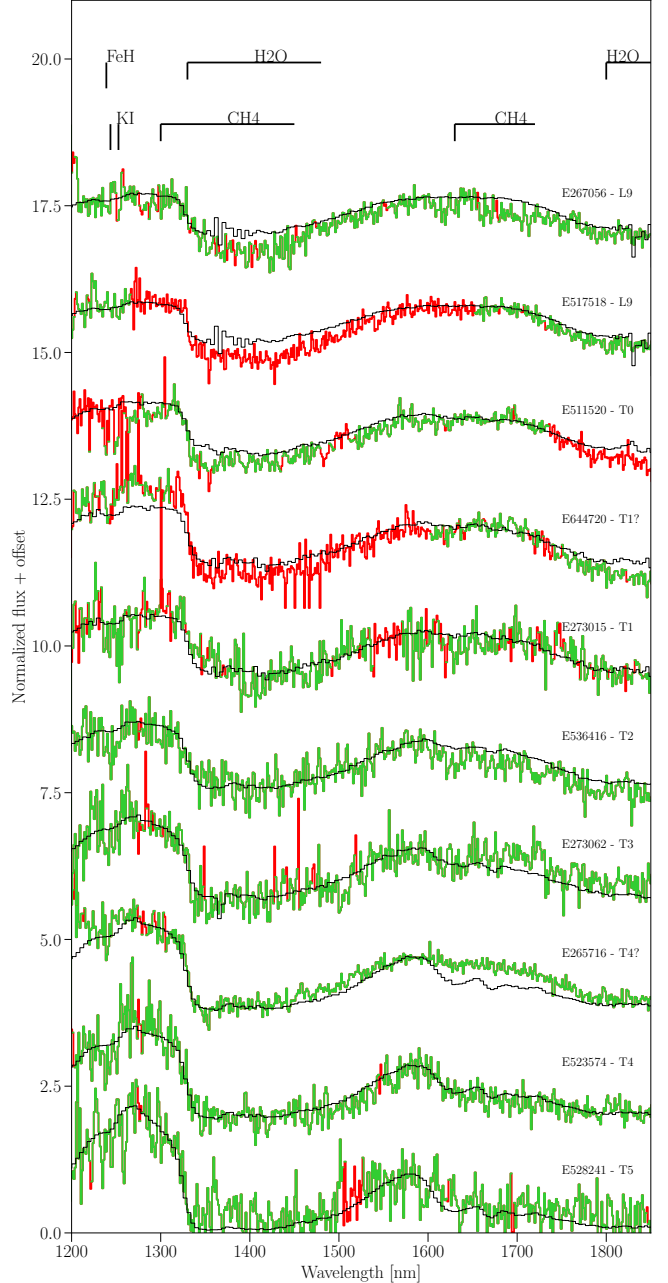


**Figure 6.** Spectra of the new late-L and T dwarfs discovered by the spectroscopic search. The flux is normalized at 1600 nm. The green lines represent the spectra with  $NDITH > 2$  and the red lines indicate the values with  $QUALITY < 0.7$ . The black lines are the standard templates (references in Appendix A).

by A. Mohandas et al. (2025). These objects are included in Table 7 (Appendix C) with the reference indicated next to the alias.

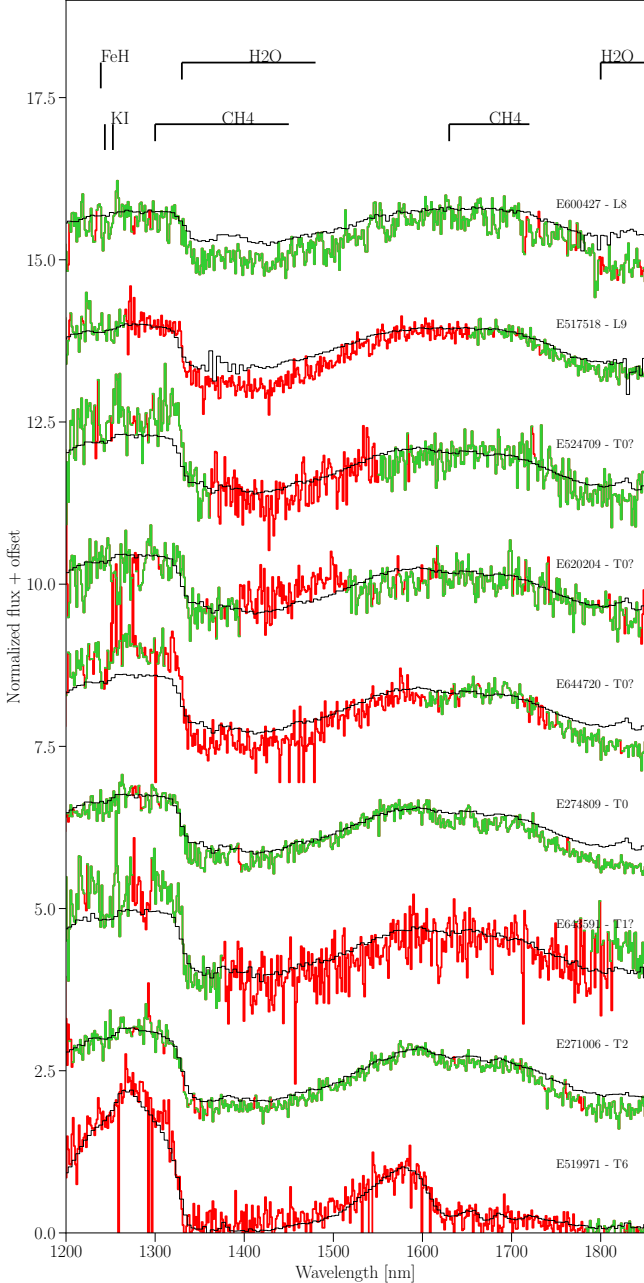


**Figure 7.** Spectra of the new late-L and T dwarfs discovered by Žerjal’s et al. (in prep.) and classified by us (this paper). The flux is normalized at 1600 nm. The green lines represent the spectra with  $\text{NDITH} > 2$  and the red lines indicate the values with  $\text{QUALITY} < 0.7$ . The black lines are the standard templates (references in Appendix A).

### 3.4. Spectra for Žerjal’s catalog

We have confirmed and classified the brighter L- and T- type UCD candidates from M. Žerjal

et al. (2025), beginning from the redder ones in the  $I_E - Y_E$  color. To date, we have classified close to one hundred UCDs not included in Zhang’s compilation nor in the spectroscopic search, of which 7 are T dwarfs, 2 are late-L dwarfs, 40 are early L dwarfs, and  $> 35$  are late M dwarfs. This list includes some peculiar objects, such as E519971, E643591, E644720, E620204, and E524709. We are investigating their nature. Fig. 7 shows the spectra of the late L- and T-type UCDs already classified. All the new objects confirmed spectroscopically are listed in Table 8 (Appendix D).

### 3.5. Comparing the photometric and spectroscopic searches

There are six UCDs discovered by the spectroscopic search that were later found in the process of creating Žerjal’s catalog: E265716, E644720, E273015, E517518, E267056, and E271934. This overlap shows the good agreement in the selection criteria. There are also five UCDs discovered by the spectroscopic search algorithm that are not included in Žerjal’s catalog. Fig. 8 shows the  $I_E - Y_E$  and  $Y_E - H_E$  colors of the UCDs found by the two searches. The objects found exclusively in the spectroscopic search are:

**E528241:** This object is classified as a T5, is very faint in the visible ( $I_E = 27.6$ ) and has colors  $I_E - Y_E = 4$  and  $Y_E - H_E = 0$ . Even if its colors match the M. Žerjal et al. (2025) criteria it was not included in the photometric selection owing to the  $\text{SNR\_VIS}$  flag.

**E523574:** This object is classified as a T4. It is faint in the visible ( $I_E = 26.7$ ), with a color  $Y_E - H_E = 0.3$ . It was not included in the photometric selection because of the  $\text{vis\_det}$  flag in VIS data. Thus, its color  $I_E - Y_E = 5.3$  has to be taken with caution. The spectrum of this object is also included in Fig. 3.

**E273062:** This object is classified as a T3 and the flags (`det_quality_flag`, `flag_vis`, `flag_y`, and `flag_h`) for the images are activated, so the color values have to be treated with caution.

**E536416:** This object is classified as a T2, is faint in the visible ( $I_E = 25.4$ ), with colors  $I_E - Y_E = 3.8$  and  $Y_E - H_E = 0.6$ . It was not included in the photometric selection because of the ellipticity filtering flag.

**E644720:** This object classified as a T1? owing to its peculiar spectrum. It is relatively bright in the visible ( $I_E = 23.2$ ), with colors  $I_E - Y_E = 3.0$  and  $Y_E - H_E = 0.5$ . It was filtered out from the photometric selection because of the `mumax_minus_mag` value.

From these objects we note that the main limitation is the quality of the images and derived data, given that the colors and filtering parameters are based on these data. It is worth to mention that E265716, the T4? object discussed in Sect. 3.3, is included in both the spectroscopic search and the photometric catalog. Its color values are:  $I_E - Y_E = 3.9$  and  $Y_E - H_E = 0.7$ .

There are four objects selected by the photometric search that were not identified by the spectroscopic search:

**E600427:** This object is an L8 dwarf that has  $PJ-JH$  and  $PH-JH$  values below the minimum ( $>0.6$  and  $>0.5$ , respectively).

**E620204:** This object is a peculiar T0 dwarf that also has  $PJ-JH$  and  $PH-JH$  values below the minimum, owing in this case to the presence of artifacts or contamination around 1400 nm.

**E519971:** This object is a T6 dwarf that was filtered out because of the presence of artifacts at different wavelengths producing NaN values in the search results.

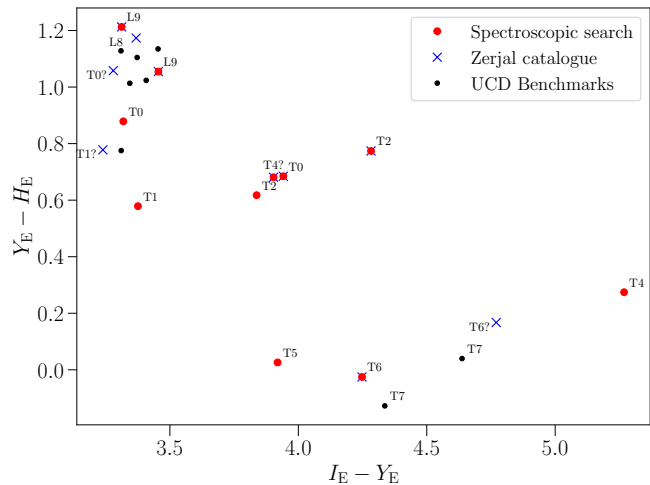


**Figure 8.**  $Y_E - H_E$  vs.  $I_E - Y_E$  color diagram as in M. Žerjal et al. (2025) with the late L- and T-type UCDs. The objects found by the spectroscopic search are plotted using the red circles, the UCD benchmarks using the black circles and the ones confirmed from Žerjal’s catalog using blue crosses. The symbol overlap means that the object is found in more than one list.

**E524709:** This object is a peculiar T0 dwarf that was filtered out owing to the presence of artifacts or contamination around 1400 nm.

#### 4. PRELIMINARY *EUCLID* UCD TEMPLATES

Spectra obtained with *Euclid* have the advantage of being free from telluric absorption bands. The large number of objects of every spectral type that we are finding and classifying provides an opportunity to create new UCD templates observed with *Euclid* from space. From the available spectra, we combined the best spectra of every spectral subtype to create such templates. Fig. 9 shows the first step in this direction, a comparison of the *Euclid* combined spectra with ground-based standard templates (black lines; references in Appendix A). Note the differences in the regions of the telluric absorption bands. These templates are the result of the combination by median of more than 10 spectra for the spectral types M7, M8, L0,

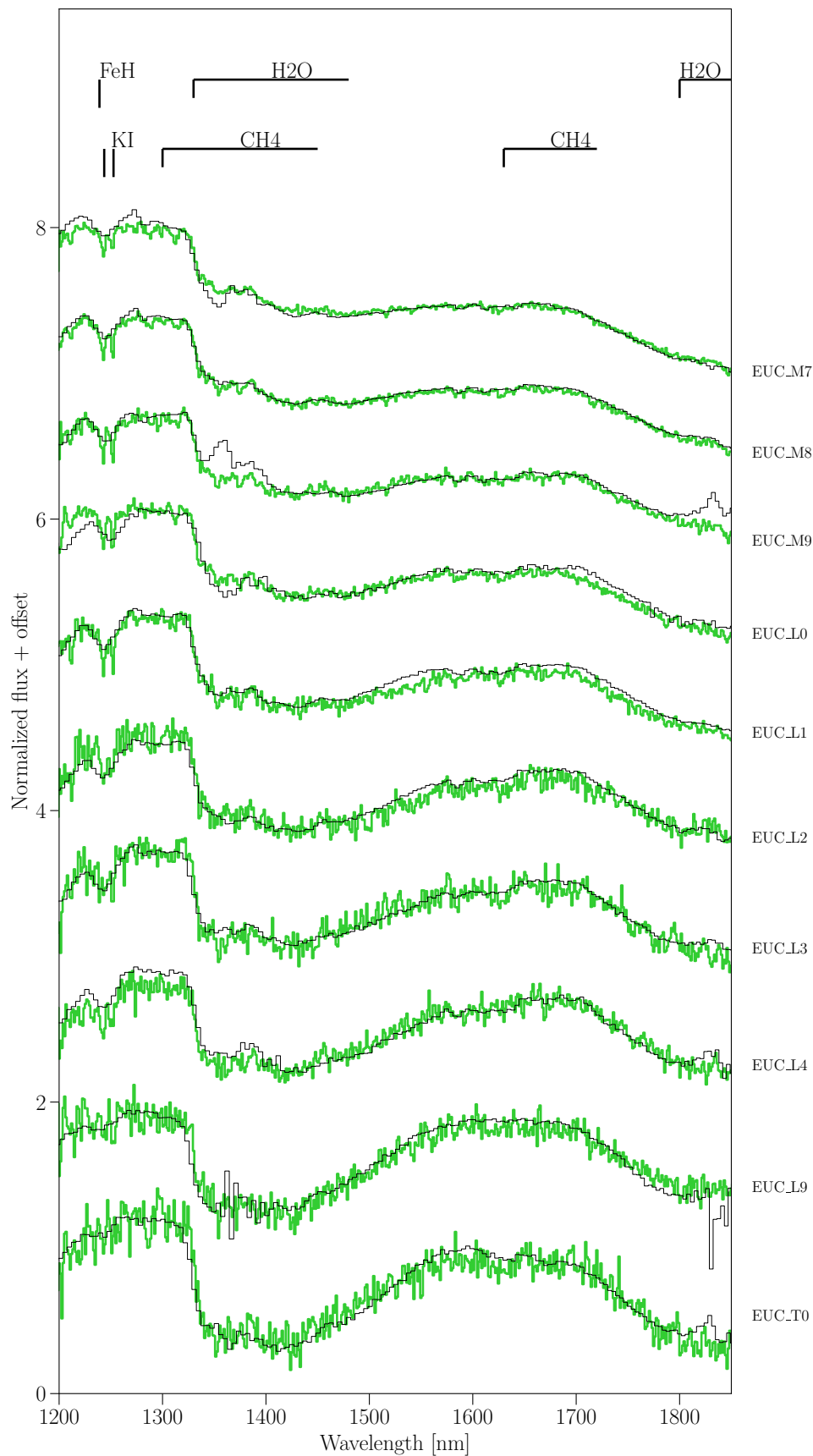


**Figure 9.** Preliminary templates (green lines) obtained from the combination by median of multiple *Euclid* spectra. The flux is normalized at 1600 nm. Each spectrum is named using "EUC" plus its spectral type. The black lines are the standard templates of the same spectral type (references in Appendix A).

**Table 3.** Preliminary templates.

Alias	Number of spectra	$T_{\text{eff}}$ (k)
EUC_T0	3	$1536^{+93}_{-59}$
EUC_L9	3	$1453^{+61}_{-129}$
EUC_L4	3	$1504^{+71}_{-139}$
EUC_L3	3	$1705^{+54}_{-118}$
EUC_L2	7	$1799^{+61}_{-51}$
EUC_L1	10	$2031^{+140}_{-32}$
EUC_L0	14	$2264^{+108}_{-37}$
EUC_M9	5	$2264^{+123}_{-51}$
EUC_M8	24	$2376^{+96}_{-35}$

NOTE—The second column indicates the number of spectra combined to obtain the template. The estimation of effective temperature ( $T_{\text{eff}}$ ) is described in Sect. 5.1

and L1. The rest of templates have a smaller number (see Table 3), thus the result is noisier. Future data releases will allow us to improve these templates by combining a larger number of spectra.

## 5. SPECTRAL ANALYSIS

### 5.1. Effective temperature determination

We determined the effective temperature ( $T_{\text{eff}}$ ) for objects with a spectral type equal or later than M8. For this, we adopted the same deep transfer learning approach presented by P. Mas-Buitrago et al. (2024), using a combination of autoencoder and convolutional neural network architectures, and tailored it to the low-resolution domain. The autoencoder models are trained on a synthetic grid, based on the **Sonora Elf Owl** models (S. Mukherjee et al. 2024), and then fine-tuned using our sample of *Euclid* UCD spectra. An in-depth discussion of the adaptation of our methodology to the low-resolution domain is presented by Mas-Buitrago et al. (in prep.).

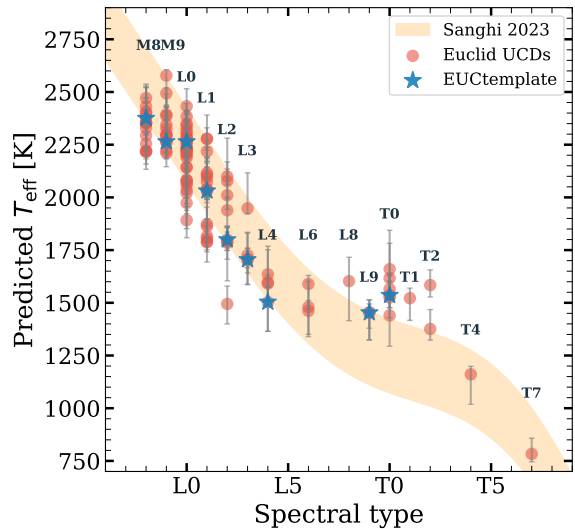


**Figure 10.** Predicted effective temperatures as a function of spectral classification for individual UCDs (red circles) and *Euclid* UCD templates (blue stars; see Sect. 4). The shaded orange area indicates the semi-empirical relation and RMS scatter derived by (A. Sanghi et al. 2023, see Fig. 16) for field UCDs.

Figure 10 shows the relationship of the derived  $T_{\text{eff}}$  values with the spectral classification from Section 3.1. The full list of measurements can be found in Table 9 (Appendix E). We also include the  $T_{\text{eff}}$  of the available *Euclid* UCD templates (which are not affected by artifacts, see Table 3 and Sect. 4). The values for the UCDs earlier than L7 are consistent with the semi-empirical measurements by A. Sanghi et al. (2023), also shown in the Figure. For the L-T transition, the predicted effective temperatures seem to be higher than those from A. Sanghi et al. (2023), showing a different profile up to T2. Beyond that, the agreement is again very good. Future observations and data releases will increase the number of objects and, with the incorporation of the missing spectral subtypes, we will be able to confirm this behavior.

### 5.2. Spectral indices

We measured the  $\text{CH}_4\text{-}J$ ,  $\text{CH}_4\text{-}H$ , and  $\text{H}_2\text{O-H}$  NIR spectral indices defined by A. J. Bur-

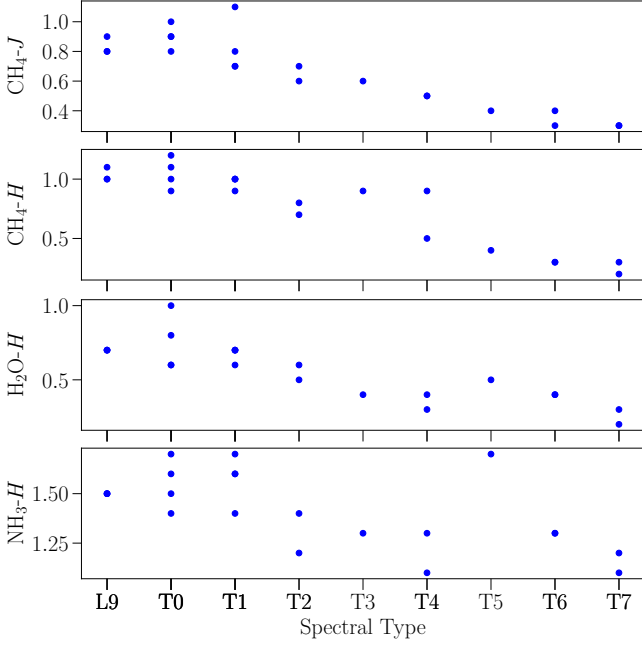


**Figure 11.** Spectral indices for late L- and T-type UCDs. The three top panels show the  $\text{CH}_4\text{-}J$ ,  $\text{CH}_4\text{-}H$ , and  $\text{H}_2\text{O-H}$  NIR spectral indices defined by A. J. Burgasser et al. (2006). The bottom panel shows the  $\text{NH}_3\text{-}H$  spectral index as defined by E. L. Martín et al. (2021).

gasser et al. (2006) for UCDs with spectral types later than L8. Fig. 11 shows how the values of these indices decrease with respect to the spectral type, in good agreement with the behavior found by A. J. Burgasser et al. (2006), and other works (see e.g. E. C. Martín et al. 2017; N. Lodieu et al. 2018).

We also measured the  $\text{NH}_3\text{-}H$  spectral index that was redefined by E. L. Martín et al. (2021) anticipating *Euclid* low spectral resolution. This index is an indicator of the absorption of ammonia in late T and Y-type UCDs. We include earlier subtypes to investigate the dispersion of values obtained with *Euclid* spectra.

### 5.3. KI absorption doublet

NISP spectral range includes the region of the KI absorption doublet at 1243.6 / 1252.6 nm (air wavelength), and the spectral resolution is good enough to resolve the two lines. This

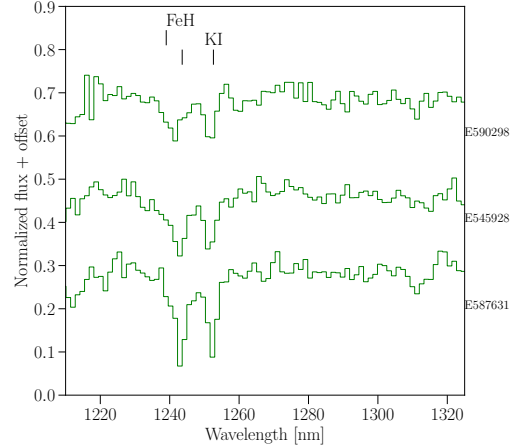


**Figure 12.** Example of different strengths in the KI absorption doublet at 1243.6 / 1252.6 nm (air wavelength) for three M8 dwarfs from Q1.

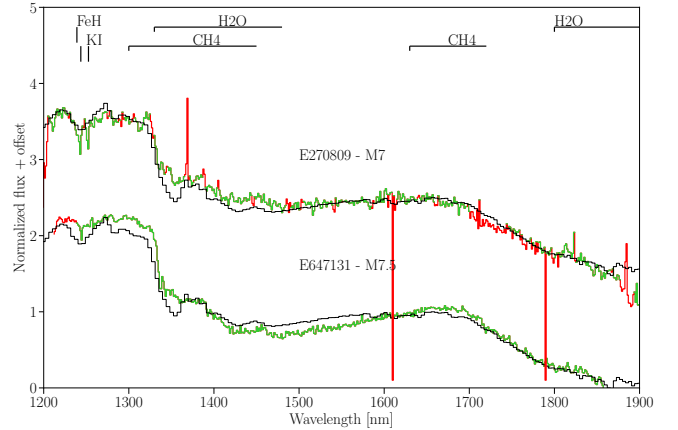


**Figure 13.** Comparison of old- and young-object spectra, both obtained with *Euclid*. Note the absence of KI absorption doublet in the lower spectrum, which corresponds to a young population. The flux is normalized at 1600 nm. E270809 spectrum is included in Q1 data of EDF-N, while that of E647131, a young object from ERO-02 regions, is taken from Dominguez-Tagle et al. (in prep.). The black lines represent the M7 standard template (A. J. Burgasser et al. 2008).

potassium doublet is a known spectral feature that increases its depth with high gravity and therefore is related to age (R. O. Gray & C. Corbally 2009). Fig. 12 shows an example of three M8 dwarfs from Q1 with different strengths

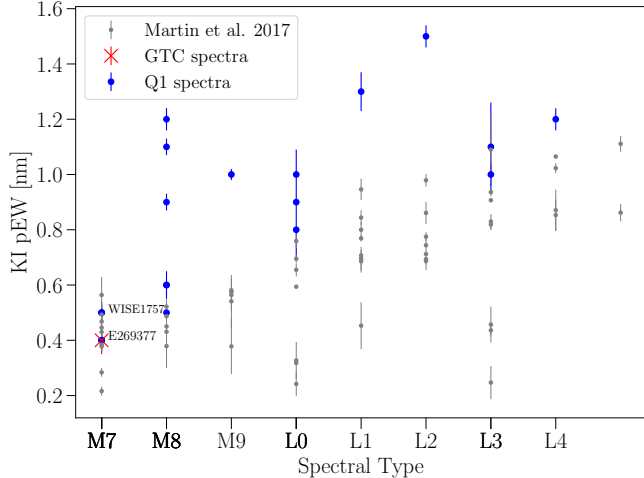


**Figure 14.** KI 1252.6 nm pseudo EWs as a function of the spectral type for objects later than M7 (blue circles; listed in Table 4). The red symbol shows the pEW for WISEA J175730.71+674138.4 (E269377 observed previously with GTC by J. Y. Zhang et al. (2024)). The grey dots represent the field UCDs from E. C. Martin et al. (2017).

in the potassium doublet. Given the different properties of the stellar populations in the EDFs and in the ERO-02 fields (E. Martín et al. 2024), we can compare old and young UCD populations. Fig. 13 shows two M7 objects as an example, E270809 from the EDF-N and E647131, a young object from the ERO-02 regions. The latter spectrum is taken from Dominguez-Tagle et al. (in prep.). The potassium doublet is strong in object E270809 whereas it is not present in E647131, a UCD from a young population. E647131 spectrum was extracted using our own code, also described in Dominguez-Tagle et al. (in prep.).

We measured the pseudo equivalent width (pEW) of the KI absorption line 1252.6 nm in the spectra of 20 dwarfs that present the KI absorption doublet region not affected by artifacts. This list includes dwarfs from M7 to L4, and the results are presented in Table 4. To measure the pEW we deblend the two potassium lines and used a window of 20 nm for the pseudo continuum out of the line region. We do not

estimate the pEW for the line at 1243.6 nm because it could be blended with an FeH feature at 1239 nm, which increases through the late-M dwarfs to early-L dwarfs (K. N. Allers & M. C. Liu 2013). Fig. 14 shows the pEW values as a function of the spectral type. Object E269377 (WISEA J175730.71+674138.4) was observed with GTC/EMIR by J. Y. Zhang et al. (2024, see Sect. 2.1), and measurements from both spectra measured in the same manner are included in the figure. The difference between both measurements, 0.1 nm is considerably larger than the uncertainties. Other comparisons are needed to verify any systematics. Fig. 14 includes the estimations for the field UCDs reported by E. C. Martin et al. (2017) plotted as gray dots. These pEW values are lower than those for Q1 data (from M8 to L2), although they present a similar scatter and follow the same correlation with respect to the spectral type. Other authors show similar results (see e.g. K. N. Allers & M. C. Liu 2013; N. Lodieu et al. 2018; A. J. Burgasser et al. 2025).

The KI 1252.6 nm absorption line could also allow to estimate radial velocities, within the limits of the NISP low spectral resolution and calibration errors. The measurements of the wavelength accuracy reported by Y. Euclid Collaboration: Copin et al. (2025) indicate that  $> 80\%$  of the occurrences are below 0.25 nm. From this value, the minimum  $3\sigma$  reliable velocity estimate is  $180 \text{ km s}^{-1}$ . Therefore, we do not aim to give an absolute value for the radial velocity, but to identify any object whose radial velocity deviates significantly from that of the rest of objects by comparing their  $KI$  ( $\lambda - \lambda_0$ ) values. Table 4 and Fig. 15 show the results. The figure is split into three panels, one per field. The objects in EDF-N and EDF-S present a dispersion of 0.4 and 0.5 nm RMS, respectively, which is larger than the typical wavelength accuracy reported by Y. Euclid Collaboration: Copin et al. (2025). The maximum

**Table 4.** KI 1252.6 nm measurements for selected objects

Alias	SpT	KI pEW (nm)	KI ( $\lambda - \lambda_0$ ) (nm)	Field
E576081	L4	$1.19 \pm 0.04$	$0.58 \pm 0.08$	S
E270698	L3	$1.09 \pm 0.16$	$-0.60 \pm 0.08$	N
E574238	L3	$1.03 \pm 0.04$	$-0.01 \pm 0.14$	S
E619358	L2	$1.48 \pm 0.04$	$-0.60 \pm 0.07$	S
E609567	L1	$1.28 \pm 0.07$	$-0.76 \pm 0.21$	S
E524930	L0	$1.02 \pm 0.09$	$0.55 \pm 0.25$	F
E265832	L0	$0.92 \pm 0.01$	$-0.14 \pm 0.03$	N
E266937	L0	$0.77 \pm 0.11$	$-0.55 \pm 0.38$	N
E638486	M9	$0.99 \pm 0.02$	$-0.42 \pm 0.06$	S
E529572	M8	$0.87 \pm 0.03$	$-0.83 \pm 0.07$	F
E545928	M8	$1.13 \pm 0.03$	$-0.20 \pm 0.07$	F
E274793	M8	$1.17 \pm 0.04$	$-0.10 \pm 0.07$	N
E658543	M8	$0.53 \pm 0.02$	$-0.15 \pm 0.04$	S
E590298	M8	$0.56 \pm 0.05$	$-0.34 \pm 0.08$	S
E587631	M8	$0.63 \pm 0.01$	$0.26 \pm 0.10$	S
E273794	M7	$0.37 \pm 0.02$	$-0.06 \pm 0.23$	N
E270809	M7	$0.39 \pm 0.01$	$-0.08 \pm 0.10$	N
E269034	M7	$0.50 \pm 0.04$	$-1.20 \pm 0.09$	N
WISE1757	M7	$0.38 \pm 0.04$	$-0.45 \pm 0.05$	N
E269377	M7	$0.48 \pm 0.02$	$0.07 \pm 0.14$	N
E661338	M7	$0.46 \pm 0.03$	$-0.82 \pm 0.19$	S

NOTE—The fifth column N, F, and S letters refer to EDF-N, EDF-F, and EDF-S, respectively.

difference between two objects in the EDF-S is 1.4 nm, that would be more than  $330 \text{ km s}^{-1}$ . E269034, located in EDF-N, deviates by 1.1 nm ( $265 \text{ km s}^{-1}$ ) from the main group of objects in the same field. Further observations, either from ground-base telescopes or future visits of *Euclid* to these fields are needed to confirm these measurements. In the latter case, they will gradually improve the SNR, the wavelength calibration, and hence, the KI measurements.

## 6. CONCLUSIONS

We searched Q1 data for the UCD candidates from Zhang’s compilation and confirmed 224

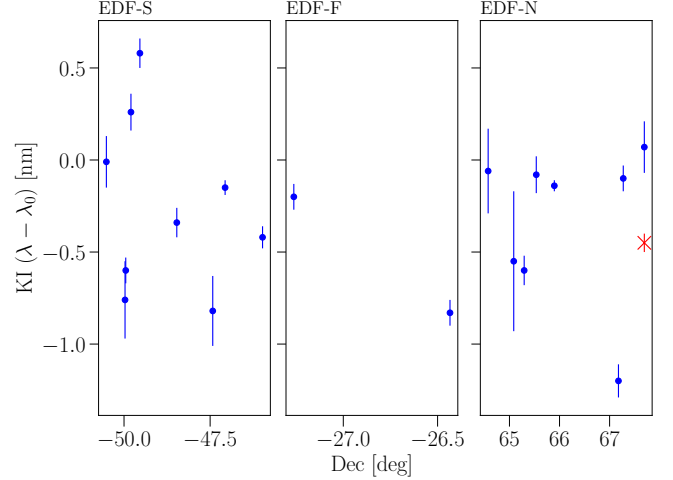


**Figure 15.** KI 1252.6 nm observed wavelength shift for the objects listed in Table 4. They are plotted as a function of their declination to group them per field. Left, mid, and right panels correspond the EDF-S, EDF-F, and EDF-N, respectively. The red symbol shows the wavelength shift for WISEA J175730.71+674138.4 (E269377 observed previously with GTC by [J. Y. Zhang et al. 2024](#)).

objects. We selected 60 UCD benchmarks from this list to be the reference for the photometric selection criteria. The list includes 38 late M dwarfs, 19 L dwarfs, and 3 T dwarfs.

We searched for late-L and T-type UCDs directly in Q1 spectra and discovered 10 objects (8 T dwarfs and 2 late-L dwarfs).

Out of 5300 candidates in Žerjal’s catalog, we have (to date) confirmed close to one hundred UCDs that were not included in Zhang’s compilation, nor in the spectroscopic search. We compared the photometric and spectroscopic searches offering hints as to why some of them were not identified by the photometric selection.

In total, we discovered and classified 15 T dwarfs and 4 late-L dwarfs, combining the photometric and spectroscopic searches.

We created a preliminary list of *Euclid* UCD templates from M7 to T0, that can be used as a reference for the future search and classification of candidates.

We demonstrated that NISP’s sensitivity is sufficient to get a useful spectrum of UCDs down to magnitude  $J_{2MASS} \sim 19$  from a single visit to a field or ROS. We investigated the capabilities of *Euclid* to study the physical properties of UCDs by their spectral features, specifically  $\text{H}_2\text{O}$ ,  $\text{CH}_4$ , and  $\text{NH}_3$  indices and the pEW of the reddest potassium line in the  $J$  band.

This paper is only a first step in the study of *Euclid* UCDs and will be improved with each subsequent data release in terms of number of objects and analysis quality, as the survey will gain 2 magnitudes in depth upon completion (Y. Euclid Collaboration: Mellier et al. 2024).

#### ACKNOWLEDGMENTS

We are grateful to T. Dupuy for his suggestions in an early version of the paper. We thank P. Schneider for the style suggestions and T. Mahoney for the English grammar corrections. Funding for CDT, MŽ, NS, ELM, and TS was provided by the European Union (ERC Advanced Grant, SUBSTELLAR, project number 101054354). The authors wish to acknowledge the contribution of the IAC High-Performance Computing support team and hardware facilities to the results of this research. PMB and ES acknowledge financial support from the Agencia Estatal de Investigación (AEI/10.13039/501100011033) of the Ministerio de Ciencia e Innovación through project PID2020-112949GB-I00 (Spanish Virtual Observatory <https://svo.cab.inta-csic.es>). PMB acknowledges support from the Instituto Nacional de Técnica Aeroespacial through grant PRE-OVE. PC acknowledges financial support from the Spanish Virtual Observatory project funded by the Spanish Ministry of Science and Innovation/State Agency of Research MCIN/AEI/10.13039/501100011033 through grant PID2020-112949GB-I00. NPB is funded by Vietnam National Foundation for Science and Technology Develop-

ment (NAFOSTED) under grant number 103.99-2020.63. This research has benefited from the SpeX Prism Spectral Libraries, maintained by Adam Burgasser at <http://www.browndwarfs.org/spexprism>. This research has made use of the SIMBAD database (Wenger et al., 2000), the Aladin sky atlas (Bonnarel et al., 2000), and the VizieR catalogue access tool developed and operated at CDS, Strasbourg, France. This work has made use of the *Euclid* Quick Release Q1 data from the *Euclid* mission of the European Space Agency (ESA), 2025, <https://doi.org/10.57780/esa-2853f3b>. This work has made use of the Early Release Observations (ERO) data from the *Euclid* mission of the European Space Agency (ESA), 2024, <https://doi.org/10.57780/esa-qmocz3>. The authors acknowledge the Euclid Consortium, the European Space Agency, and a number of agencies and institutes that have supported the development of *Euclid*, in particular the Agenzia Spaziale Italiana, the Austrian Forschungsförderungsgesellschaft funded through BMK, the Belgian Science Policy, the Canadian Euclid Consortium, the Deutsches Zentrum für Luft- und Raumfahrt, the DTU Space and the Niels Bohr Institute in Denmark, the French Centre National d’Etudes Spatiales, the Fundação para a Ciência e a Tecnologia, the Hungarian Academy of Sciences, the Ministerio de Ciencia, Innovación y Universidades, the National Aeronautics and Space Administration, the National Astronomical Observatory of Japan, the Nederlandse Onderzoekschool Voor Astronomie, the Norwegian Space Agency, the Research Council of Finland, the Romanian Space Agency, the State Secretariat for Education, Research, and Innovation (SERI) at the Swiss Space Office (SSO), and the United Kingdom Space Agency. A complete and detailed list is available on the *Euclid* web site ([www.euclid-ec.org](http://www.euclid-ec.org)).

*Facilities:* *Euclid* space mission, GTC, VLT

*Software:* SPLAT (A. J. Burgasser & Splat Development Team 2017), astropy (Astropy Collaboration et al. 2013, 2018, 2022), TOPCAT (M. B. Taylor 2005)

## APPENDIX

## A. UCD STANDARD TEMPLATES

**Table 5.** Standard templates used in this paper

SpT	Name	SpT reference	Data reference
M6.0	Wolf 359	J. D. Kirkpatrick et al. (1991)	A. J. Burgasser et al. (2008)
M7.0	VB 8	J. D. Kirkpatrick et al. (1991)	A. J. Burgasser et al. (2008)
M8.0	VB 10	J. D. Kirkpatrick et al. (1991)	A. J. Burgasser et al. (2004)
M9.0	LHS 2924	J. D. Kirkpatrick et al. (1991)	A. J. Burgasser & M. W. McElwain (2006)
L0.0	2MASS J0345432+254023	J. D. Kirkpatrick et al. (1999)	A. J. Burgasser & M. W. McElwain (2006)
L1.0	2MASSW J1439284+192915	J. D. Kirkpatrick et al. (1999)	A. J. Burgasser et al. (2004)
L2.0	Kelu-1	J. D. Kirkpatrick et al. (1999)	A. J. Burgasser et al. (2007)
L3.0	2MASSW J1506544+132106	J. E. Gizis et al. (2000)	A. J. Burgasser (2007)
L4.0	2MASS J21580457-1550098	J. D. Kirkpatrick et al. (2008)	D. C. Bardalez Gagliuffi et al. (2014)
L5.0	SDSS J083506.16+195304.4	K. Chiu et al. (2006)	K. Chiu et al. (2006)
L6.0	2MASSI J1010148-040649	K. L. Cruz et al. (2003)	I. N. Reid et al. (2006)
L7.0	2MASSI J0103320+193536	H. Bouy et al. (2022)	K. L. Cruz et al. (2003)
L8.0	2MASSW J1632291+190441	J. D. Kirkpatrick et al. (1999)	A. J. Burgasser et al. (2004)
L9.0	DENIS-P J0255-4700	J. D. Kirkpatrick et al. (2008)	A. J. Burgasser et al. (2006)
T0.0	SDSS J120747.17+024424.8	S. L. Hawley et al. (2002)	D. L.Looper et al. (2007)
T1.0	SDSSp J083717.22-000018.3	A. J. Burgasser et al. (2006)	A. J. Burgasser et al. (2006)
T2.0	SDSSp J125453.90-012247.4	A. J. Burgasser et al. (2006)	A. J. Burgasser et al. (2004)
T3.0	2MASS J12095613-1004008	A. J. Burgasser et al. (2006)	A. J. Burgasser et al. (2004)
T4.0	2MASSI J2254188+312349	A. J. Burgasser et al. (2006)	A. J. Burgasser et al. (2004)
T5.0	2MASS J15031961+2525196	A. J. Burgasser et al. (2006)	A. J. Burgasser et al. (2004)
T6.0	SDSSp J162414.37+002915.6	A. J. Burgasser et al. (2006)	A. J. Burgasser et al. (2004)
T7.0	2MASSI J0727182+171001	A. J. Burgasser et al. (2006)	A. J. Burgasser et al. (2004)
T8.0	2MASSI J0415195-093506	A. J. Burgasser et al. (2006)	A. J. Burgasser et al. (2004)
T9.0	UGPS J072227.51-054031.2	A. J. Burgasser et al. (2006)	A. J. Burgasser & Splat Development Team (2017)

## B. UCD BENCHMARKS

Description in Sect. 3.2

**Table 6.** Descriptive version of the “Full list of UCD benchmarks” table.

Alias	SpT	<i>Euclid</i> ID	RA(J2000)	Dec(J2000)	$J_{2MASS}$
E581332	T7	-581332495491830038	03:52:32.0	-49:10:58.8	17.8
E597913	T7	-597913643476826162	03:59:09.9	-47:40:57.4	18.1
E607287	T0	-607287223470778395	04:02:54.9	-47:04:40.2	18.9
E576081	L4	-576081983495392396	03:50:26.0	-49:32:21.3	18.0
E638441	L4	-638441224479182813	04:15:22.6	-47:55:05.8	17.7
E593750	L4	-593750792477935412	03:57:30.0	-47:47:36.7	18.3
E594656	L3	-594656949486432578	03:57:51.8	-48:38:35.7	18.3
E574238	L3	-574238742505125019	03:49:41.7	-50:30:45.0	17.8
E603529	L3	-603529747469286537	04:01:24.7	-46:55:43.2	18.1

NOTE—This table is published in its entirety in the electronic edition of the *Astrophysical Journal*. A portion is shown here for guidance regarding its form and content.

## C. LIST OF OBJECTS FOUND BY THE SPECTROSCOPIC SEARCH

Description in Sect. 2.2

**Table 7.** Late-L and T dwarfs found by the spectroscopic search

Alias (Ref.)	SpT	<i>Euclid</i> ID	RA(J2000)	Dec(J2000)	$I_E$	$Y_E$	$J_E$	$H_E$
E581332 <sup>1</sup>	T7	-581332495491830038	03:52:32.0	-49:10:58.8	24.3	20.0	19.5	20.1
E597913 <sup>1</sup>	T7	-597913643476826162	03:59:09.9	-47:40:57.4	24.8	20.2	19.8	20.2
E266485 <sup>2</sup>	T6	2664850113649936423	17:45:56.4	+64:59:37.1	24.7	20.4	20.0	20.5
E528241	T5	-528241075263163744	03:31:17.8	-26:18:58.9	27.6	23.6	23.2	23.6
E523574	T4	-523574860290315045	03:29:25.8	-29:01:53.4	26.7	21.4	20.9	21.1
E265716 <sup>4</sup>	T4?	2657163304658383990	17:42:51.9	+65:50:18.2	24.4	20.5	20.1	19.8
E273062	T3	2730620775659672177	18:12:14.9	+65:58:02.0	24.0	20.9	20.6	20.5
E536416	T2	-536416224285940430	03:34:34.0	-28:35:38.6	25.4	21.5	21.2	20.9
E271006 <sup>3</sup>	T2	2710066793674540980	18:04:01.6	+67:27:14.8	24.6	20.3	19.9	19.5
E644720 <sup>4</sup>	T1?	-644720877461587627	04:17:53.3	-46:09:31.5	22.9	19.5	19.2	18.9
E273015 <sup>4</sup>	T1	2730150213677979458	18:12:03.6	+67:47:52.6	23.2	20.2	19.8	19.7
E511520	T0	-511520903274482292	03:24:36.5	-27:26:53.6	22.9	19.6	19.1	18.7
E274809 <sup>3</sup>	T0	2748094058670347269	18:19:14.3	+67:02:05.0	23.3	19.4	19.0	18.7
E517518 <sup>4</sup>	L9	-517518361295768184	03:27:00.4	-29:34:36.5	23.3	19.9	19.3	18.8
E267056 <sup>4</sup>	L9	2670569747654000953	17:48:13.7	+65:24:00.3	24.0	20.7	20.0	19.4
E271934 <sup>4, 5</sup>	L4?	2719340730667146696	18:07:44.2	+66:42:52.8	23.8	20.4	19.9	19.5

NOTE— The object alias with no notes are discoveries by the spectroscopic search, the rest are: (1) two already cited in Zhang’s compilation (and references therein); (2) one cited in [G. N. Mace et al. \(2013\)](#); (3) two already found by [M. Žerjal et al. \(2025\)](#); (4) six discovered by the spectroscopic search that were later found in the process of creating Žerjal’s catalog; (5) one also included in [A. Mohandas et al. \(2025\)](#). The magnitudes are from [M. Žerjal et al. \(2025\)](#).

#### D. SPECTROSCOPICALLY CONFIRMED UCDS FROM ŽERJAL’S CATALOG

Description in Sect. 3.4

#### E. EFFECTIVE TEMPERATURES ESTIMATIONS

Description in Sect. 5.1.

#### REFERENCES

- Allers, K. N., & Liu, M. C. 2013, *ApJ*, 772, 79,  
doi: [10.1088/0004-637X/772/2/79](#)
- Astropy Collaboration, Robitaille, T. P., Tollerud, E. J., et al. 2013, *A&A*, 558, A33,  
doi: [10.1051/0004-6361/201322068](#)
- Astropy Collaboration, Price-Whelan, A. M., Sipőcz, B. M., et al. 2018, *AJ*, 156, 123,  
doi: [10.3847/1538-3881/aabc4f](#)
- Astropy Collaboration, Price-Whelan, A. M., Lim, P. L., et al. 2022, *ApJ*, 935, 167,  
doi: [10.3847/1538-4357/ac7c74](#)
- Aussel, H., et al. 2025, *A&A*, submitted
- Bardalez Gagliuffi, D. C., Burgasser, A. J., Gelino, C. R., et al. 2014, *ApJ*, 794, 143,  
doi: [10.1088/0004-637X/794/2/143](#)
- Bouy, H., Tamura, M., Barrado, D., et al. 2022, *A&A*, 664, A111,  
doi: [10.1051/0004-6361/202243850](#)
- Burgasser, A. J. 2007, *ApJ*, 659, 655,  
doi: [10.1086/511027](#)

**Table 8.** Descriptive version of the “Spectroscopically confirmed late-L and T dwarfs from Žerjal’s catalog” table.

Alias	SpT	<i>Euclid</i> ID	RA(J2000)	Dec(J2000)
E519971	T6	-519971822278279190	03:27:59.3	-27:49:40.5
E271006	T2	2710066793674540980	18:04:01.6	+67:27:14.8
E643591	T1?	-643591214457657250	04:17:26.2	-45:45:56.6
E274809	T0	2748094058670347269	18:19:14.3	+67:02:05.0
E644720	T0?	-644720877461587627	04:17:53.3	-46:09:31.5
E620204	T0?	-620204558458613530	04:08:04.9	-45:51:40.9
E524709	T0?	-524709228264023336	03:29:53.0	-26:24:08.4
E517518	L9	-517518361295768184	03:27:00.4	-29:34:36.5

NOTE—This list exclude the objects found in Zhang’s compilation and in the spectroscopic search. The table is published in its entirety in the electronic edition of the *Astrophysical Journal*. A portion is shown here for guidance regarding its form and content.

**Table 9.** Descriptive version of the “Effective temperature ( $T_{\text{eff}}$ ) estimations” table.

Alias	SpT	$T_{\text{eff}}$ (K)
E581332	T7	$783^{+75}_{-37}$
E523574	T4	$1161^{+38}_{-142}$
E536416	T2	$1584^{+72}_{-57}$
E271006	T2	$1376^{+92}_{-53}$
E643591	T1	$1522^{+48}_{-105}$
E274809	T0	$1565^{+38}_{-136}$
E607287	T0	$1440^{+79}_{-146}$
E644720	T0?	$1525^{+114}_{-15}$
E524709	T0?	$1660^{+122}_{-61}$
E620204	T0?	$1617^{+227}_{-71}$
E517518	L9	$1455^{+39}_{-76}$

NOTE—This table is published in its entirety in the electronic edition of the *Astrophysical Journal*. A portion is shown here for guidance regarding its form and content.

Burgasser, A. J., Geballe, T. R., Leggett, S. K., Kirkpatrick, J. D., & Golimowski, D. A. 2006, *ApJ*, 637, 1067, doi: [10.1086/498563](https://doi.org/10.1086/498563)

Burgasser, A. J., Liu, M. C., Ireland, M. J., Cruz, K. L., & Dupuy, T. J. 2008, *ApJ*, 681, 579, doi: [10.1086/588379](https://doi.org/10.1086/588379)

Burgasser, A. J., Looper, D. L., Kirkpatrick, J. D., & Liu, M. C. 2007, *ApJ*, 658, 557, doi: [10.1086/511518](https://doi.org/10.1086/511518)

Burgasser, A. J., & McElwain, M. W. 2006, *AJ*, 131, 1007, doi: [10.1086/499042](https://doi.org/10.1086/499042)

Burgasser, A. J., McElwain, M. W., Kirkpatrick, J. D., et al. 2004, *AJ*, 127, 2856, doi: [10.1086/383549](https://doi.org/10.1086/383549)

- Burgasser, A. J., & Splat Development Team. 2017, in *Astronomical Society of India Conference Series*, Vol. 14, *Astronomical Society of India Conference Series*, 7–12, doi: [10.48550/arXiv.1707.00062](https://doi.org/10.48550/arXiv.1707.00062)
- Burgasser, A. J., Kirkpatrick, J. D., Brown, M. E., et al. 2002, *ApJ*, 564, 421, doi: [10.1086/324033](https://doi.org/10.1086/324033)
- Burgasser, A. J., Schneider, A. C., Meisner, A. M., et al. 2025, <https://arxiv.org/abs/2411.01378>
- Chiu, K., Fan, X., Leggett, S. K., et al. 2006, *AJ*, 131, 2722, doi: [10.1086/501431](https://doi.org/10.1086/501431)
- Cruz, K. L., Reid, I. N., Liebert, J., Kirkpatrick, J. D., & Lowrance, P. J. 2003, *AJ*, 126, 2421, doi: [10.1086/378607](https://doi.org/10.1086/378607)
- Cushing, M. C., Kirkpatrick, J. D., Gelino, C. R., et al. 2011, *ApJ*, 743, 50, doi: [10.1088/0004-637X/743/1/50](https://doi.org/10.1088/0004-637X/743/1/50)
- Cutri, R. M., Skrutskie, M. F., van Dyk, S., et al. 2003, *2MASS All Sky Catalog of point sources*. (Publisher)
- Delorme, P., Delfosse, X., Albert, L., et al. 2008, *A&A*, 482, 961, doi: [10.1051/0004-6361:20079317](https://doi.org/10.1051/0004-6361:20079317)
- Euclid Collaboration: Copin, Y., Fumana, M., Mancini, C., et al. 2025, *A&A*, submitted
- Euclid Collaboration: Cropper, M., Al Bahlawan, A., Amiaux, J., et al. 2024, *A&A*, accepted, arXiv:2405.13492. <https://arxiv.org/abs/2405.13492>
- Euclid Collaboration: Jahnke, K., Gillard, W., Schirmer, M., et al. 2024, *A&A*, accepted, arXiv:2405.13493. <https://arxiv.org/abs/2405.13493>
- Euclid Collaboration: Mellier, Y., Abdurro'uf, Acevedo Barroso, J., et al. 2024, *A&A*, accepted, arXiv:2405.13491. <https://arxiv.org/abs/2405.13491>
- Euclid Collaboration: Scaramella, R., Amiaux, J., Mellier, Y., et al. 2022, *A&A*, 662, A112, doi: [10.1051/0004-6361/202141938](https://doi.org/10.1051/0004-6361/202141938)
- Geballe, T. R., Knapp, G. R., Leggett, S. K., et al. 2002, *ApJ*, 564, 466, doi: [10.1086/324078](https://doi.org/10.1086/324078)
- Gizis, J. E., Monet, D. G., Reid, I. N., et al. 2000, *AJ*, 120, 1085, doi: [10.1086/301456](https://doi.org/10.1086/301456)
- Gray, R. O., & Corbally, J., C. 2009, *Stellar Spectral Classification* (Publisher)
- Hawley, S. L., Covey, K. R., Knapp, G. R., et al. 2002, *AJ*, 123, 3409, doi: [10.1086/340697](https://doi.org/10.1086/340697)
- Kirkpatrick, J. D., Henry, T. J., & Irwin, M. J. 1997, *AJ*, 113, 1421, doi: [10.1086/118357](https://doi.org/10.1086/118357)
- Kirkpatrick, J. D., Henry, T. J., & McCarthy, Jr., D. W. 1991, *ApJS*, 77, 417, doi: [10.1086/191611](https://doi.org/10.1086/191611)
- Kirkpatrick, J. D., Henry, T. J., & Simons, D. A. 1995, *AJ*, 109, 797, doi: [10.1086/117323](https://doi.org/10.1086/117323)
- Kirkpatrick, J. D., Reid, I. N., Liebert, J., et al. 1999, *ApJ*, 519, 802, doi: [10.1086/307414](https://doi.org/10.1086/307414)
- Kirkpatrick, J. D., Reid, I. N., Liebert, J., et al. 2000, *AJ*, 120, 447, doi: [10.1086/301427](https://doi.org/10.1086/301427)
- Kirkpatrick, J. D., Cruz, K. L., Barman, T. S., et al. 2008, *ApJ*, 689, 1295, doi: [10.1086/592768](https://doi.org/10.1086/592768)
- Kirkpatrick, J. D., Cushing, M. C., Gelino, C. R., et al. 2011, *ApJS*, 197, 19, doi: [10.1088/0067-0049/197/2/19](https://doi.org/10.1088/0067-0049/197/2/19)
- Le Brun, V., et al. 2025, *A&A*, submitted
- Lodieu, N., Zapatero Osorio, M. R., Béjar, V. J. S., & Peña Ramírez, K. 2018, *MNRAS*, 473, 2020, doi: [10.1093/mnras/stx2279](https://doi.org/10.1093/mnras/stx2279)
- Looper, D. L., Kirkpatrick, J. D., & Burgasser, A. J. 2007, *AJ*, 134, 1162, doi: [10.1086/520645](https://doi.org/10.1086/520645)
- Luhman, K. L. 2014, *ApJL*, 786, L18, doi: [10.1088/2041-8205/786/2/L18](https://doi.org/10.1088/2041-8205/786/2/L18)
- Luhman, K. L., Tremblin, P., Alves de Oliveira, C., et al. 2024, *AJ*, 167, 5, doi: [10.3847/1538-3881/ad0b72](https://doi.org/10.3847/1538-3881/ad0b72)
- Mace, G. N., Kirkpatrick, J. D., Cushing, M. C., et al. 2013, *ApJS*, 205, 6, doi: [10.1088/0067-0049/205/1/6](https://doi.org/10.1088/0067-0049/205/1/6)
- Martín, E., Žerjal, M., Bouy, H., et al. 2024, *A&A*, accepted, arXiv:2405.13497. <https://arxiv.org/abs/2405.13497>
- Martin, E. C., Mace, G. N., McLean, I. S., et al. 2017, *ApJ*, 838, 73, doi: [10.3847/1538-4357/aa6338](https://doi.org/10.3847/1538-4357/aa6338)
- Martin, E. L., Basri, G., Delfosse, X., & Forveille, T. 1997, *A&A*, 327, L29
- Martin, E. L., Basri, G., Zapatero-Osorio, M. R., Rebolo, R., & López, R. J. G. 1998, *ApJL*, 507, L41, doi: [10.1086/311675](https://doi.org/10.1086/311675)
- Martin, E. L., Delfosse, X., Basri, G., et al. 1999, *AJ*, 118, 2466, doi: [10.1086/301107](https://doi.org/10.1086/301107)
- Martín, E. L., Zhang, J. Y., Esparza, P., et al. 2021, *A&A*, 655, L3, doi: [10.1051/0004-6361/202142470](https://doi.org/10.1051/0004-6361/202142470)
- Mas-Buitrago, P., González-Marcos, A., Solano, E., et al. 2024, *A&A*, 687, A205, doi: [10.1051/0004-6361/202449865](https://doi.org/10.1051/0004-6361/202449865)
- Mohandas, A., Smart, R., Reylé, C., et al. 2025, *A&A*, submitted

- Mukherjee, S., Fortney, J. J., Morley, C. V., et al. 2024, *ApJ*, 963, 73, doi: [10.3847/1538-4357/ad18c2](https://doi.org/10.3847/1538-4357/ad18c2)
- Reid, I. N., Lewitus, E., Allen, P. R., Cruz, K. L., & Burgasser, A. J. 2006, *AJ*, 132, 891, doi: [10.1086/505626](https://doi.org/10.1086/505626)
- Sanghi, A., Liu, M. C., Best, W. M., et al. 2023, *Research Notes of the AAS*, 7, 194, doi: [10.3847/2515-5172/acf864](https://doi.org/10.3847/2515-5172/acf864)
- Skrutskie, M. F., Cutri, R. M., Stiening, R., et al. 2006, *AJ*, 131, 1163, doi: [10.1086/498708](https://doi.org/10.1086/498708)
- Taylor, M. B. 2005, in *Astronomical Society of the Pacific Conference Series*, Vol. 347, *Astronomical Data Analysis Software and Systems XIV*, ed. P. Shopbell, M. Britton, & R. Ebert, 29
- Žerjal, M., et al. 2025, *A&A*, submitted
- Zhang, J. Y., Lodieu, N., & Martín, E. L. 2024, *A&A*, 686, A171, doi: [10.1051/0004-6361/202348769](https://doi.org/10.1051/0004-6361/202348769)